



**HAL**  
open science

## Luminescence and mechanoluminescence of $\text{Ba}_4\text{Si}_6\text{O}_{16}:\text{Eu}^{2+}$ , RE phosphors

Alexis Duval, Yan Suffren, Mourad Benabdesselam, Patrick Houizot, Tanguy Rouxel

► **To cite this version:**

Alexis Duval, Yan Suffren, Mourad Benabdesselam, Patrick Houizot, Tanguy Rouxel. Luminescence and mechanoluminescence of  $\text{Ba}_4\text{Si}_6\text{O}_{16}:\text{Eu}^{2+}$ , RE phosphors. The Journal of Chemical Physics, 2023, 159 (13), pp.134501. 10.1063/5.0167222 . hal-04258645

**HAL Id: hal-04258645**

**<https://hal.science/hal-04258645v1>**

Submitted on 11 Dec 2023

**HAL** is a multi-disciplinary open access archive for the deposit and dissemination of scientific research documents, whether they are published or not. The documents may come from teaching and research institutions in France or abroad, or from public or private research centers.

L'archive ouverte pluridisciplinaire **HAL**, est destinée au dépôt et à la diffusion de documents scientifiques de niveau recherche, publiés ou non, émanant des établissements d'enseignement et de recherche français ou étrangers, des laboratoires publics ou privés.



Distributed under a Creative Commons Attribution - NonCommercial 4.0 International License

# Luminescence and mechanoluminescence of

## $\text{Ba}_4\text{Si}_6\text{O}_{16}:\text{Eu}^{2+}$ , *RE* phosphors

Alexis Duval<sup>1,a)</sup>, Yan Suffren<sup>2</sup>, Mourad Benabdesselam<sup>3</sup>, Patrick Houizot<sup>1</sup> and Tanguy Rouxel<sup>1,4</sup>

### AFFILIATIONS

<sup>1</sup>Glass Mechanics Lab., IPR (Institut de Physique de Rennes), UMR 6251, University of Rennes, Campus de Beaulieu, Rennes, France.

<sup>2</sup>INSA Rennes, CNRS, ISCR (Institut des Sciences Chimiques de Rennes), UMR 6226, University of Rennes, Campus de Beaulieu, Rennes, France.

<sup>3</sup>INPHYNI (Institut de Physique de Nice), UMR 7010, Côte d'Azur University, Nice, France.

<sup>4</sup>Institut Universitaire de France, Paris, France.

<sup>a)</sup>Author to whom correspondence should be addressed: [alexis.duval@univ-rennes.fr](mailto:alexis.duval@univ-rennes.fr)

### ABSTRACT

The luminescence properties of green  $\text{Ba}_4\text{Si}_6\text{O}_{16}:\text{Eu}^{2+}$ , *RE* (*RE* = Sc, Y, La-Lu except Pm) phosphors are reported. Their long-lasting phosphorescence is discussed in view of trap depths and concentrations determined from thermally stimulated luminescence experiments. A second emission band centered at 439 nm was evidenced at low temperatures, which stems from the substitution of  $\text{Eu}^{2+}$  in the two non-equivalent  $\text{Ba}^{2+}$  sites of  $\text{Ba}_4\text{Si}_6\text{O}_{16}$ . The mechanoluminescence properties of  $\text{Ba}_4\text{Si}_6\text{O}_{16}:\text{Eu}^{2+}$ , *RE* phosphors are described, and a new mechanoluminescence mechanism is proposed, in the case where *RE* =  $\text{Ho}^{3+}$  involving a trap

22 distribution from 0.694 to 0.924 eV. Mechanical loading (post UV irradiation) induces a  
23 decrease in depth of the trap distribution leading to an increase of the luminescence intensity,  
24 whereas a drop of the luminescence intensity is observed upon unloading, following the faster  
25 release of the charge carriers.

## 26 1. INTRODUCTION

27 The luminescence properties of oxides, oxynitrides and nitrides from the BaO-SiO<sub>2</sub>-Si<sub>3</sub>N<sub>4</sub>  
28 system were reported in the past few years, such as BaSi<sub>2</sub>O<sub>5</sub>:Eu<sup>2+</sup> <sup>1 2</sup> ( $\lambda_{em}$  = 500-505 nm),  
29 Ba<sub>3</sub>Si<sub>5</sub>O<sub>13- $\delta$</sub> N <sub>$\delta$</sub> :Eu<sup>2+</sup> <sup>3</sup> (broad emission bands from 400 to 620 nm), Ba<sub>5</sub>Si<sub>8</sub>O<sub>21</sub>:Eu<sup>2+</sup> <sup>4 5 6</sup>  
30 ( $\lambda_{em}$  = 473-480 nm), Ba<sub>4</sub>Si<sub>6</sub>O<sub>16</sub>:Eu<sup>2+</sup> <sup>7 8 9 10</sup> ( $\lambda_{em}$  = 496-515 nm),  $\beta$ -BaSiO<sub>3</sub>:Eu<sup>2+</sup> <sup>6 11</sup>  
31 ( $\lambda_{em}$  = 560-565 nm), Ba<sub>2</sub>SiO<sub>4</sub>:Eu<sup>2+</sup> <sup>12 13 14 15</sup> ( $\lambda_{em}$  = 503-510 nm), Ba<sub>3</sub>SiO<sub>5</sub>:Eu<sup>2+</sup> <sup>6 16 17 18 19</sup>  
32 ( $\lambda_{em}$  = 585-596 nm), BaSi<sub>2</sub>O<sub>2</sub>N<sub>2</sub>:Eu<sup>2+</sup> <sup>20 21 22</sup> ( $\lambda_{em}$  = 498-500 nm) or Ba<sub>2</sub>Si<sub>5</sub>N<sub>8</sub>:Eu<sup>2+</sup> <sup>23</sup>  
33 ( $\lambda_{em}$  = 585 nm). This chemical system offers a broad range of emission colors, ranging from  
34 blue to orange.

35 The luminescence properties of Ba<sub>4</sub>Si<sub>6</sub>O<sub>16</sub>:Eu<sup>2+</sup> were reported as early as the 60s, but were  
36 mostly studied during the last 15 years with various luminescent centers such as Eu<sup>2+</sup>, Pr<sup>3+</sup> and  
37 Ce<sup>3+</sup> <sup>8 24 25</sup>. In the crystal, the rare-earths (*RE*) substitute for Ba<sup>2+</sup> ions thanks to close ionic radii  
38 <sup>26</sup>. Its space group is *P2<sub>1</sub>/c* <sup>27</sup> ( $a = 12.477 \text{ \AA}$ ,  $b = 4.685 \text{ \AA}$ ,  $c = 13.944 \text{ \AA}$ ,  $\beta = 93.54^\circ$ ,  $Z = 2$ ),  
39 which is similar to the non-standard *P2<sub>1</sub>/a* formerly used <sup>8</sup>. Ba<sub>4</sub>Si<sub>6</sub>O<sub>16</sub>:Eu<sup>2+</sup> is a potential  
40 phosphor for applications in white light emitting diodes (*wLEDs*), but synthesis complications  
41 including mixed phases like Ba<sub>3</sub>Si<sub>5</sub>O<sub>13</sub> and Ba<sub>5</sub>Si<sub>8</sub>O<sub>21</sub> and high sintering temperatures limit its  
42 use <sup>10</sup>.

43 Ba<sub>4</sub>Si<sub>6</sub>O<sub>16</sub> exhibits an intense long-lasting phosphorescence (*LLP*) as well as  
44 elasto-mechanoluminescence (*EML*) <sup>28</sup> when doped with Eu<sup>2+</sup>, in a similar way as BaSi<sub>2</sub>O<sub>2</sub>N<sub>2</sub>.

45 Recall that elasto-mechanoluminescence is the emission of light resulting from an elastic

46 deformation. This phenomenon has recently aroused great interest, because of potential  
47 applications of mechanoluminescent materials for energy storage or as stress sensors <sup>29</sup>. The  
48 BaO-SiO<sub>2</sub> binary diagram shows a glass-forming region with a BaO content from 20 to  
49 50 mol. % <sup>30</sup>, along with congruent crystallization at given BaO contents. This allowed the  
50 formation of Ba<sub>4</sub>Si<sub>6</sub>O<sub>16</sub>:Eu<sup>2+</sup>, Ho<sup>3+</sup>-containing glass-ceramics exhibiting *EML* thanks to  
51 uniformly dispersed active crystals <sup>28</sup>. In our previous work (ref. <sup>28</sup>), we have reported  
52 mechanoluminescence in a new glass-ceramic material mainly consisting of  
53 Ba<sub>4</sub>Si<sub>6</sub>O<sub>16</sub>:Eu<sup>2+</sup>, *RE* crystalline phase. In this preliminary work, we focused on the choice for  
54 the *RE* co-dopant and we have reported the first mechanical testing results, which revealed  
55 significant differences with the behavior of SrAl<sub>2</sub>O<sub>4</sub>:Eu<sup>2+</sup>, Dy<sup>3+</sup>. The present manuscript  
56 provides an in-depth investigation of the role of the co-dopant in the e<sup>-</sup> trapping energetics and  
57 in the physics of the luminescence mechanism. *LLP* behavior as well as *EML* properties are  
58 related to the characteristics of electron traps within the active crystalline phase. Trap depths  
59 and concentrations were determined from thermally stimulated luminescence experiments.  
60 Experiments with different loading rates and loading modes allow to propose a mechanism of  
61 the *EML* phenomenon in the particular crystal.

## 62 2. EXPERIMENTAL

63 Ba<sub>4</sub>Si<sub>6</sub>O<sub>16</sub>:Eu<sup>2+</sup>, *RE* crystals were synthesized starting from dried BaCO<sub>3</sub> (Sigma-Aldrich  
64 99 %), Gd<sub>2</sub>O<sub>3</sub>, Lu<sub>2</sub>O<sub>3</sub>, Dy<sub>2</sub>O<sub>3</sub>, Sc<sub>2</sub>O<sub>3</sub>, Eu<sub>2</sub>O<sub>3</sub> (Sigma-Aldrich 99.9 %), SiO<sub>2</sub> (Sigma-Aldrich  
65 99.5 %), Pr<sub>2</sub>O<sub>3</sub>, Sm<sub>2</sub>O<sub>3</sub> (Fischer 99.9 %), Tb<sub>4</sub>O<sub>7</sub> (Fischer 99.998 %), Tm<sub>2</sub>O<sub>3</sub> (Alfa Aesar  
66 99.9 %), Yb<sub>2</sub>O<sub>3</sub>, La<sub>2</sub>O<sub>3</sub>, CeO<sub>2</sub>, Nd<sub>2</sub>O<sub>3</sub> (Rhône-Poulenc 99.99 %), Y<sub>2</sub>O<sub>3</sub> (Acros 99.99 %), and  
67 Ho<sub>2</sub>O<sub>3</sub>, Er<sub>2</sub>O<sub>3</sub> (Rhône-Poulenc 99.999 %). Three series of Ba<sub>4</sub>Si<sub>6</sub>O<sub>16</sub>:Eu<sup>2+</sup>, *RE* crystals were  
68 studied, with i) a fixed cationic composition: 35 Ba – 60 Si – 3 Eu – 2 *RE* for each *RE*, ii)  
69

70 varying  $\text{Eu}^{2+}:\text{RE}$  ratio for  $\text{RE} = \text{Pr}^{3+}$  or  $\text{Ho}^{3+}$ , and iii) varying  $\text{Eu}^{2+}:\text{RE}$  quantity for  $\text{RE} = \text{Ho}^{3+}$ .  
71 Stoichiometric amounts were weighted and grounded during 15 minutes in ethanol in an agate  
72 mortar, and then fired 6 h at 1300 °C in an alumina crucible under a  $\text{N}_2:\text{H}_2 = 94:6$  reducing  
73 atmosphere. Each specimen was grounded into a fine powder.

74 The X-ray diffraction (XRD) patterns were collected using a PANalytical X'pert Pro  
75 diffractometer using Cu-K $\alpha$  radiation (1.5418 Å).

76 Solid-state excitation and emission spectra were recorded using a Horiba Jobin-Yvon  
77 Fluorolog III fluorescence spectrometer equipped with a Xe lamp operating at 450 W, a  
78 UV-vis-nearIR photomultiplier (Hamamatsu R928, sensitivity 190 – 860 nm), or a  
79 Horiba Jobin-Yvon FluoroMax-4 Plus fluorescence spectrometer equipped with a Xe lamp  
80 operating at 150 W and a UV-vis photomultiplier (Hamamatsu R928, sensitivity  
81 190 – 860 nm). The luminescence spectra were realized on powder samples placed inside the  
82 solid-sample holder fixed in 30° rotation and blocked by a quartz blade.

83 Emission and excitation spectra of  $\text{Ba}_4\text{Si}_6\text{O}_{16}:\text{Eu}^{2+}$ ,  $\text{Ho}^{3+}$  were recorded from 77 to 300 K in  
84 quartz cuvettes with an optical cryostat (OptistatCF from Oxford Inst.) coupled to a liquid  
85 nitrogen bath under a  $\text{N}_2$  atmosphere, and from 300 to 380 K in a solid holder using a F-3004  
86 Jobin-Yvon heating Peltier module.

87 Appropriate filters were used to remove the residual excitation laser light, the Rayleigh  
88 scattered light and associated harmonics from the spectra. All spectra were corrected for the  
89 instrumental response function.

90 Solid-state UV-visible absorption measurements were obtained with a PerkinElmer Lambda  
91 650 spectrometer using a 60 mm integrated sphere.

This is the author's peer-reviewed, accepted manuscript. It has not been certified for publication. PLEASE CITE THIS ARTICLE AS DOI: 10.1063/5.0167222

92 Quantum yield measurements were recorded using a G8 GMP integrating sphere according to:  
93  $\Phi = (E_c - E_a)/(L_a - L_c)$ , where  $E_c$  is the integrated emission spectrum of the sample,  $E_a$  is the  
94 integrated “blank” emission spectrum,  $L_a$  is the “blank” absorption, and  $L_c$  is the sample  
95 absorption at the excitation wavelength. Samples were introduced in specific capillaries for a  
96 G8 integrating sphere, and placed directly inside the integrating sphere.

97 Rapid luminescence decays were measured directly with the fluorescence spectrometer  
98 connected to an additional time-correlated single photon counting (*TCSPC*) module and a  
99 360 nm pulsed delta diode. Lifetimes and quantum yields are the averages of three independent  
00 measurements.

01 Luminance, expressed in  $\text{mcd}\cdot\text{m}^{-2}$ , was measured on a  $1.5\text{ cm}^2$  sample pellet using a Konica  
02 Minolta LS-150 luminancemeter with an integration time of 3 s under UV irradiation  
03 ( $\lambda_{exc} = 365\text{ nm}$ ) in a lab-made black box. The working distance between the luminancemeter  
04 and the pellet surface was 45 cm. The irradiation was realized with a lab-made source  
05 constituted by 1 LED CUN66B1B from Roithner at 365 nm plugged in a Keysight  
06 Technologies E36104B benchtop power supply that provides the desired current (mA) and  
07 voltage (V). The incident beam angle is  $30^\circ$  with respect to the normal of the pellet surface and  
08 the distance *LED*-sample is 12 cm. In order to avoid saturation the current was fixed at 90 mA  
09 and the voltage at 3.32 V, with an effective power of  $0.57\text{ mW}\cdot\text{cm}^{-2}$ .

10 Thermally stimulated luminescence (*TSL*) experiments were performed from 293 to 573 K with  
11 a heating rate of  $1\text{ K}\cdot\text{s}^{-1}$ . The delay between the end of the UV illumination and reading was  
12 40 s. During heating, the *TSL* signal was detected by means of a UV-visible photomultiplier  
13 tube.

14 *LLP* emission spectra were collected by an optical multichannel analyzer (*OMA*), consisting of  
15 a multimode optical fiber connected to an integrated spectrograph equipped with a CCD array

This is the author's final proof. Please refer to the final version of the article for the most accurate information. For more information, please contact the publisher. DOI: 10.1063/1.5167222

16 covering the range 200-1100 nm. An appropriate grating covering the 200-1100 nm range was  
17 used.

18 *LLP* and *EML* experiments were performed on powder/epoxy composites, where each  
19  $\text{Ba}_4\text{Si}_6\text{O}_{16}:\text{Eu}^{2+}$ , *RE* crystal was mixed with an epoxy resin (obtained by mixing EPOFIX resin  
20 Struers and EPOFIX hardener Struers with a 90:10 concentration by weight) with a final powder  
21 content of 20 wt. %. Mechanical tests were carried out on disks using a Shimadzu-AGS-X  
22 testing machine with a 10 kN load cell and a SiC pusher. The stress  $\sigma$  induced at the center of  
23 a disk made in the composite material (epoxy + ceramic powder) during the diametral  
24 compression test is expressed as  $\sigma = \frac{2P}{\pi dh}$ , where  $P$  is the load,  $d$  the diameter (11.5 mm) and  $h$   
25 the height (6 mm) of the disk <sup>31</sup>. The *LLP* intensity and the *EML* intensity were quantified  
26 consistently using a Zyla 5.5 sCMOS Andor Technology high sensitivity camera, by irradiating  
27 each sample for 2 minutes using a 365 nm handheld UV light with an effective power of  
28 1.22 mW·cm<sup>-2</sup> prior to mechanical loading.

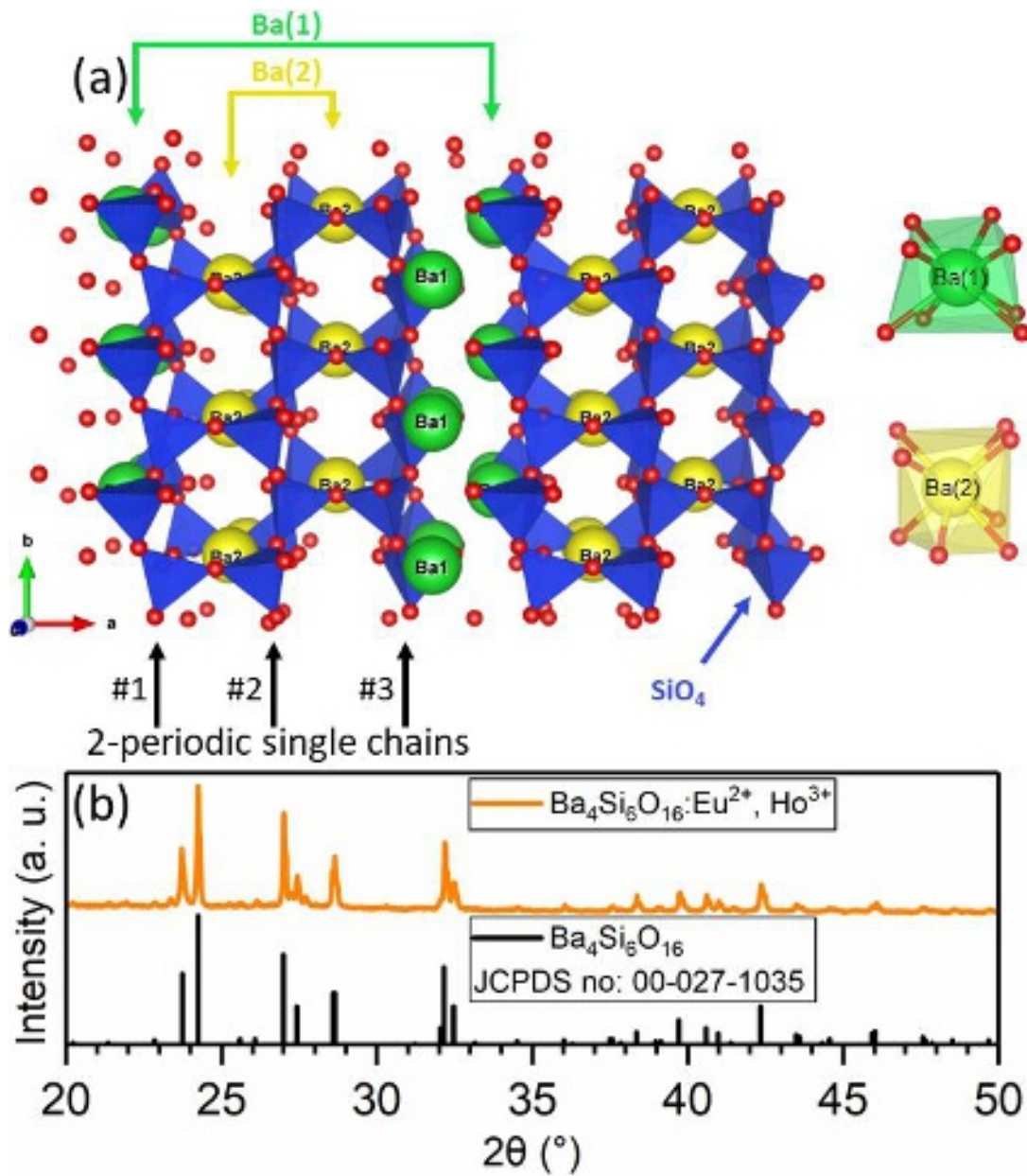
### 30 3. RESULTS AND DISCUSSION

#### 31 3.1 Luminescence properties of $\text{Ba}_4\text{Si}_6\text{O}_{16}:\text{Eu}^{2+}$ , *RE*

32 In a  $\text{Ba}_4\text{Si}_6\text{O}_{16}$  crystal,  $\text{SiO}_4$  tetrahedra are corner-sharing to form 2-periodic single chains <sup>27</sup>  
33 FIG. 1 (a). Three single chains are linked into triple chains, running along [010] with a 21  
34 symmetry, therefore forming 6-membered rings <sup>5 7</sup>. Two non-equivalent VIII-coordinated  $\text{Ba}^{2+}$   
35 sites exist in  $\text{Ba}_4\text{Si}_6\text{O}_{16}$ , where Ba(1) is located in between two triple chains while Ba(2) is  
36 located between two single chains.

37 Three series of  $\text{Ba}_4\text{Si}_6\text{O}_{16}:\text{Eu}^{2+}$ , *RE* crystals were designed as to study both the incidence of the  
38 various *RE* co-doping, the *Eu:RE* ratio and the *Eu+RE* quantity on the luminescence properties.

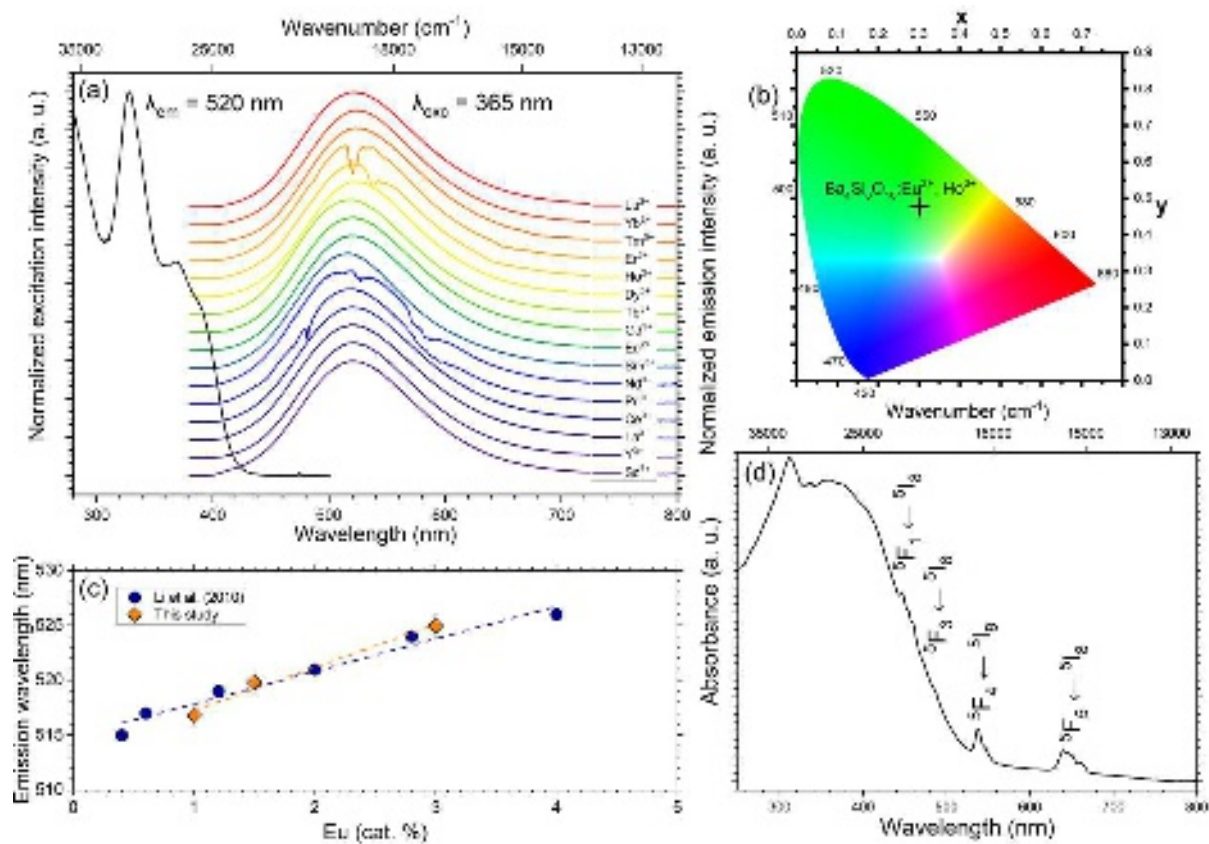
39 XRD patterns confirmed the sole crystallization of  $\text{Ba}_4\text{Si}_6\text{O}_{16}$  in each sample FIG. 1 (b). The  
40 excitation spectra were similar with a change of  $RE$ , extending up to 420 nm with a maximum  
41 at  $\lambda_{max} = 329$  nm FIG. 2 (a). Just like  $\text{Ba}_5\text{Si}_8\text{O}_{21}:\text{Eu}^{2+}$ ,  $\text{Dy}^{3+}$ <sup>5</sup>, such broad excitation spectra  
42 make it possible to activate  $\text{Ba}_4\text{Si}_6\text{O}_{16}:\text{Eu}^{2+}$ ,  $RE$  phosphors simply through sunlight irradiation.



43  
44 **FIG. 1.** (a) Crystal structure of  $\text{Ba}_4\text{Si}_6\text{O}_{16}$ . Green, yellow, and blue polyhedra correspond to  
45 Ba(1), Ba(2), and Si-based polyhedra respectively. The local coordination of the Ba(1) and



46 Ba(2) sites with the oxygen atoms (red) is shown (b) Typical *XRD* pattern of a  $\text{Ba}_4\text{Si}_6\text{O}_{16}:\text{Eu}^{2+}$ ,  
 47 *RE* crystal, here when  $RE = \text{Ho}^{3+}$  (orange), and the standard *XRD* pattern of  $\text{Ba}_4\text{Si}_6\text{O}_{16}$  (black).  
 48 An excitation wavelength of 365 nm was chosen for the following measurements to remain  
 49 consistent with the *EML* experiments discussed later in the article. The emission spectra consist  
 50 of a broad emission band from 400 to 700 nm characteristic of the  $4f^65d^1 \rightarrow 4f^7$  transition of  
 51  $\text{Eu}^{2+}$ , with a maximum ranging from 516 to 526 nm. While its position is *RE*-dependent, no  
 52 conclusions could be obtained regarding its trend. All  $\text{Ba}_4\text{Si}_6\text{O}_{16}:\text{Eu}^{2+}$ , *RE* crystals exhibited a  
 53 green emission, with CIE coordinates  $x = 0.302$ ,  $y = 0.478$  when  $RE = \text{Ho}^{3+}$  FIG. 2 (b).



54  
 55 **FIG. 2.** (a) Excitation spectrum of  $\text{Ba}_4\text{Si}_6\text{O}_{16}:\text{Eu}^{2+}$ ,  $\text{Ho}^{3+}$ , and emission spectra of  
 56  $\text{Ba}_4\text{Si}_6\text{O}_{16}:\text{Eu}^{2+}$ , *RE* crystals (b) CIE chromaticity coordinates of  $\text{Ba}_4\text{Si}_6\text{O}_{16}:\text{Eu}^{2+}$ ,  $\text{Ho}^{3+}$  (c)  
 57 Dependence of the emission wavelength on the europium concentration in  $\text{Ba}_4\text{Si}_6\text{O}_{16}:\text{Eu}^{2+}$ ,  $\text{Ho}^{3+}$

58 crystals with a fixed Eu:Ho ratio, and in  $\text{Ba}_{4-y}\text{Eu}_y\text{Si}_6\text{O}_{15.85}\text{N}_{0.1}$  crystals <sup>7</sup> (d) Absorption  
59 spectrum of  $\text{Ba}_4\text{Si}_6\text{O}_{16}:\text{Eu}^{2+}, \text{Ho}^{3+}$ .

60 In the literature, the  $\lambda_{max}$  position of the broad emission band of  $\text{Ba}_4\text{Si}_6\text{O}_{16}:\text{Eu}^{2+}$ , *RE* crystals  
61 ranges from 494 up to 526 nm. Indeed, its position is slightly redshifted when the europium  
62 concentration is increased <sup>7</sup>. Here, the emission maximum of  $\text{Ba}_4\text{Si}_6\text{O}_{16}:\text{Eu}^{2+}, \text{Ho}^{3+}$  crystals with  
63 a fixed Eu:Ho ratio but with increasing europium concentrations from 1 to 3 cat. % increases  
64 from 517 to 525 nm FIG. 2 (c). Typically,  $\text{Eu}^{2+}$  concentrations from 0.08 to 1.5 cat. % lead to  
65 emission maxima ranging from 495 to 505 nm <sup>9 10 32 33</sup>, while higher concentrations up to  
66 4 cat. % lead to a maximum emission at 526 nm <sup>7</sup>. Hence, the reported emission color of  
67  $\text{Ba}_4\text{Si}_6\text{O}_{16}:\text{Eu}^{2+}$ , *RE* phosphors ranges from bluish-green to green, and can easily be tuned by  
68 choosing the right *RE* co-doping as well as  $\text{Eu}^{2+}$  concentration. The higher the  $\text{Eu}^{2+}$   
69 concentration is and the smaller the distance between the europium ions becomes, which means  
70 that the probability of energy transfer from higher-energy 5d levels  $\text{Eu}^{2+}$  ions to lower-energy  
71 5d levels  $\text{Eu}^{2+}$  ions increases, resulting in the end in an emission band shifting towards longer  
72 wavelength <sup>9</sup>.

73 Several absorption peaks were observed when *RE* =  $\text{Pr}^{3+}, \text{Nd}^{3+}, \text{Ho}^{3+}$ , or  $\text{Er}^{3+}$ , with positions at  
74 538, 547, and 638 nm in the case of  $\text{Ho}^{3+}$  corresponding to transitions from the ground state  $^5\text{I}_8$   
75 to  $^5\text{F}_4, ^5\text{S}_2$ , and  $^5\text{F}_5$  respectively <sup>34</sup>. The absorption spectrum of  $\text{Ba}_4\text{Si}_6\text{O}_{16}:\text{Eu}^{2+}, \text{Ho}^{3+}$  revealed  
76 both the broad absorption band of  $\text{Eu}^{2+}$  at short wavelength (< 400 nm), as well as various  $\text{Ho}^{3+}$   
77 intraconfigurational transitions FIG. 2 (d). The absorption and the quantum efficiency were  
78 estimated at  $79 \pm 10\%$  and  $17 \pm 10\%$  respectively with  $\lambda_{exc} = 365$  nm. Li *et al.* <sup>7</sup> reported a  
79 similar absorption (80 %) but a considerably higher quantum efficiency (46 %) in  
80  $\text{Ba}_{3.8}\text{Eu}_{0.2}\text{Si}_6\text{O}_{15.85}\text{N}_{0.1}$ .

This is the author's peer-reviewed, accepted manuscript. It may be subject to change before the final version. It is not to be distributed, copied, or used in any form without the permission of the publisher. PLEASE CITE THIS ARTICLE AS DOI: 10.1063/5.0167222

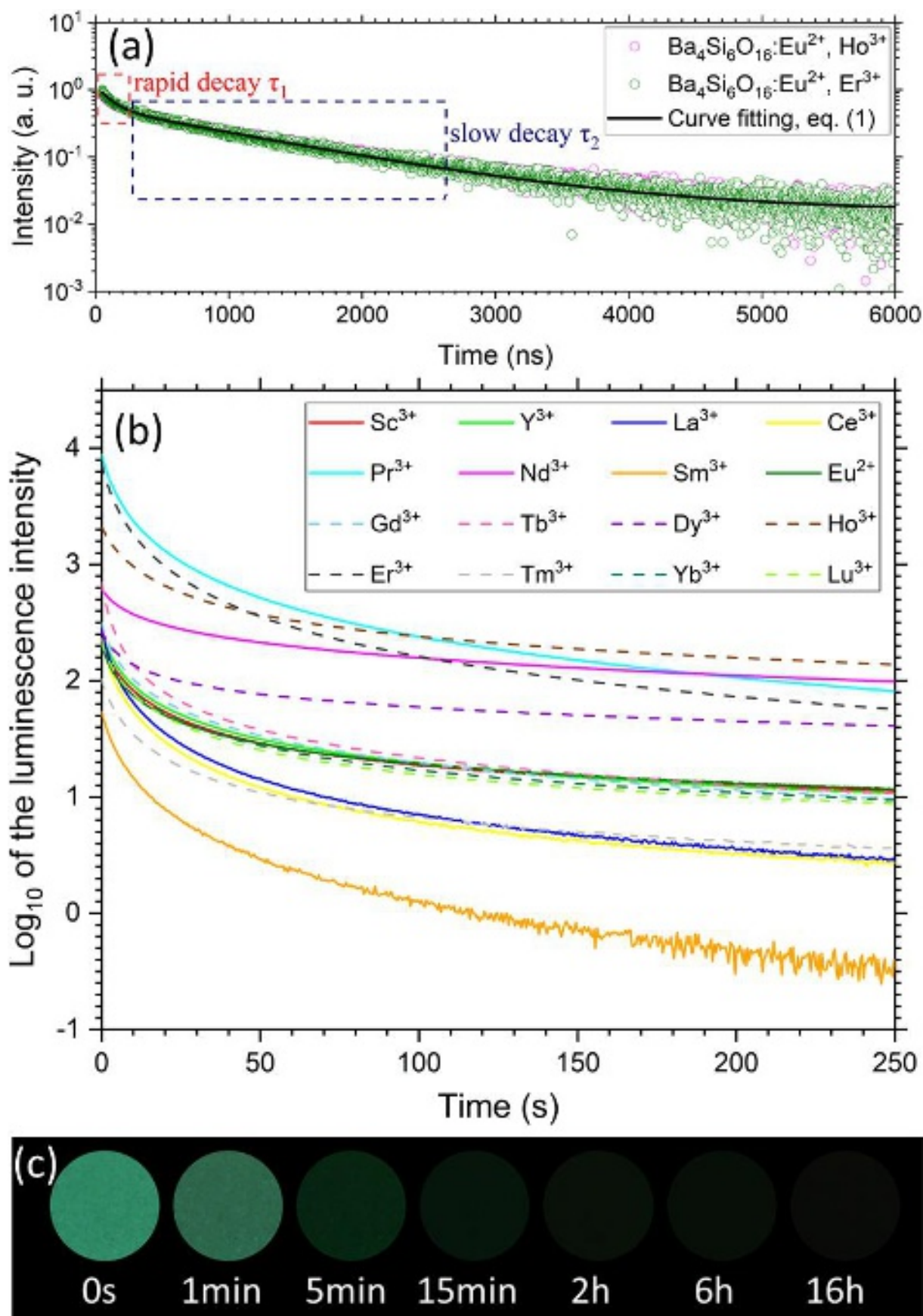
81 The luminescence decay was studied over a duration of 6000 ns for  $RE = \text{Ho}^{3+}$  and  $\text{Er}^{3+}$ . It can  
82 be fitted using equation (1):

$$83 \quad I(t) = A_1 \exp\left(-\frac{t}{\tau_1}\right) + A_2 \exp\left(-\frac{t}{\tau_2}\right) \quad (1)$$

84 Where  $I(t)$  is the luminescence intensity at a given time  $t$ ,  $A_1$  and  $A_2$  are constants, and  $\tau_1$  and  
85  $\tau_2$  are time constants describing the luminescence decay. Two regimes are observed in the  
86 beginning for a duration of about 200 ns : a rapid one at  $t < 200$  ns followed by a slower one,  
87 corresponding respectively to  $\tau_1 = 0.107 \pm 0.002 \mu\text{s}$  and  $\tau_2 = 1.140 \pm 0.004 \mu\text{s}$  FIG. 3 (a),  
88 suggesting that in both cases the luminescent center is  $\text{Eu}^{2+}$  while the  $RE$  act as sensitizers.  
89 Yang *et al.*<sup>10</sup> also identified two lifetimes in  $\text{Ba}_4\text{Si}_6\text{O}_{16}:\text{Eu}^{2+}$ ,  $RE$  crystals when  $RE = \text{Eu}^{2+}$ ,  $\text{Dy}^{3+}$ ,  
90 or  $\text{Ho}^{3+}$ , however these lifetimes are significantly larger than those reported here ( $\tau_1 = 4 \mu\text{s}$  and  
91  $\tau_2 = 30.3 \mu\text{s}$ ). In addition, Chen *et al.*<sup>8</sup> observed a decrease of the effective decay time with an  
92 increase of the europium content in  $\text{Ba}_{3.86-y}\text{Si}_6\text{O}_{16}:0.07\text{Ce}^{3+}, 0.07\text{Li}^+, y\text{Eu}^{2+}$ , which suggests that  
93 a variation of the  $\text{Eu}^{2+}:\text{RE}$  ratio and/or  $\text{Eu}^{2+}+\text{RE}$  quantity induces a visible change of the  
94 specimens lifetime. This was attributed to energy transfers between  $RE^{3+}$  co-dopants and  $\text{Eu}^{2+}$ .  
95 However, the kinetics of the  $LLP$  decay depends significantly on the selected  $RE$  FIG. 3 (b).  
96 While the steady-state luminescence ( $SSL$ ) intensity is roughly similar whatever the  $RE$ , the  
97  $LLP$  intensity changes significantly. For example, it is increased by two orders of magnitude as  
98  $\text{Ho}^{3+}$  substitutes  $\text{Sm}^{3+}$ . The  $RE$  leading to the highest  $LLP$  intensity at times smaller than 250 ns  
99 are, in descending order,  $\text{Ho}^{3+}$ ,  $\text{Nd}^{3+}$ ,  $\text{Pr}^{3+}$  and  $\text{Er}^{3+}$ . The luminescence of  $\text{Ba}_4\text{Si}_6\text{O}_{16}:\text{Eu}^{2+}$ ,  $\text{Ho}^{3+}$   
00 is visible to the naked eye beyond a day after the excitation source is stopped. FIG. 3 (c) displays  
01 photographs at various times of the  $LLP$  decay in the case of  $\text{Ba}_4\text{Si}_6\text{O}_{16}:\text{Eu}^{2+}$ ,  $\text{Ho}^{3+}$ .

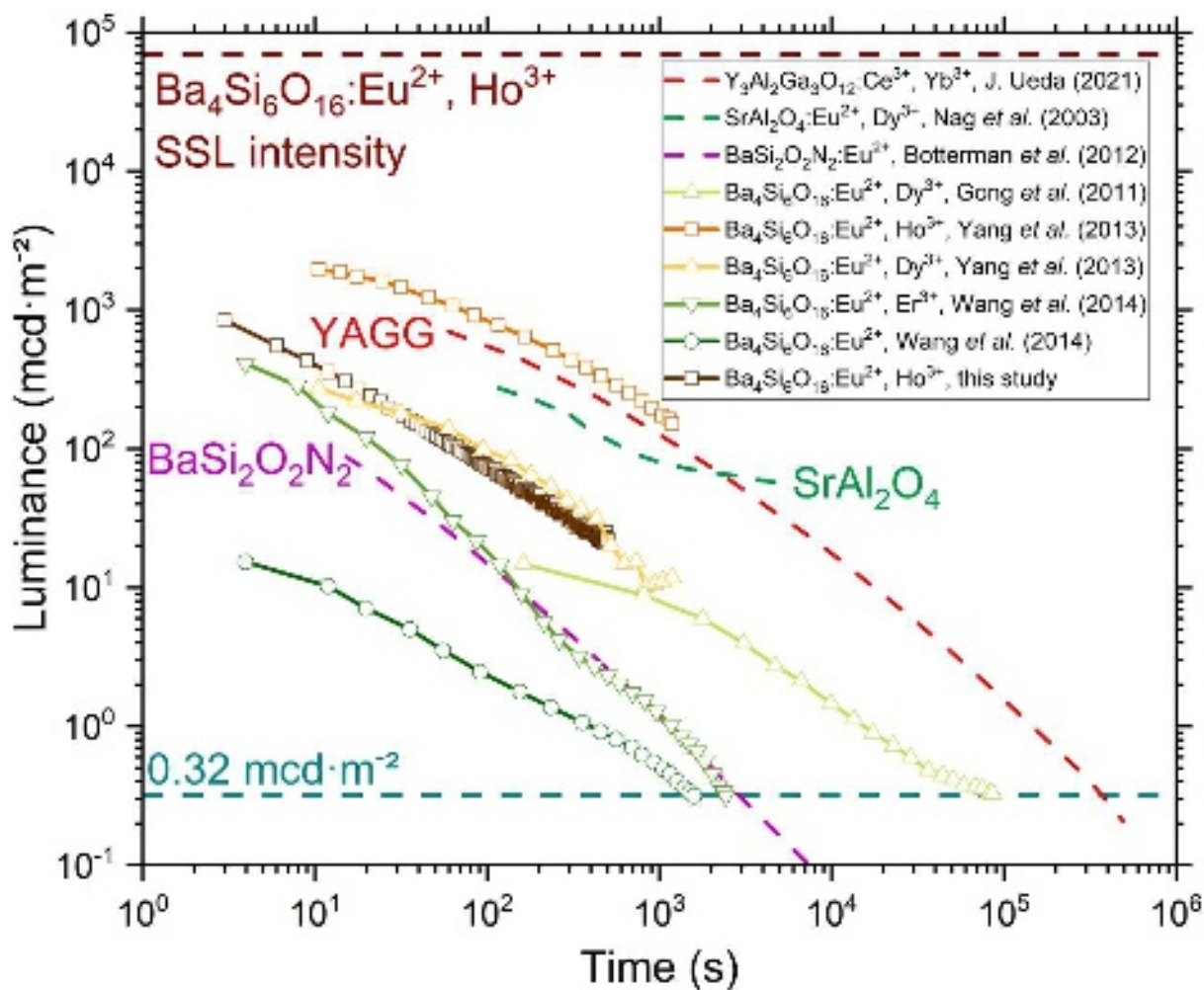
This is the author's peer reviewed, accepted manuscript. Please cite this article as: DOI: 10.1063/1.5016722

This is the author's pre-proof reviewed, accepted manuscript. However, the online version of record will be different from this version once it has been copyedited and typeset.  
PLEASE CITE THIS ARTICLE AS DOI: 10.1063/5.0167222



03 **FIG. 3.** (a) Rapid-decay of  $\text{Ba}_4\text{Si}_6\text{O}_{16}:\text{Eu}^{2+}$ ,  $RE$  crystals for  $RE = \text{Ho}^{3+}$  or  $\text{Er}^{3+}$  (b)  $LLP$  decay of  
 04  $\text{Ba}_4\text{Si}_6\text{O}_{16}:\text{Eu}^{2+}$ ,  $RE$  crystals (c) Photographs of  $\text{Ba}_4\text{Si}_6\text{O}_{16}:\text{Eu}^{2+}$ ,  $\text{Ho}^{3+}$  taken at various times  
 05 after the excitation source is stopped, excited beforehand 2 minutes by a 365 nm UV light. Each  
 06 disk is 1 cm wide.

07 The afterglow intensity of  $\text{Ba}_4\text{Si}_6\text{O}_{16}:\text{Eu}^{2+}$ ,  $\text{Ho}^{3+}$  drops by two orders of magnitude as soon as  
 08 the excitation source is stopped FIG. 4. It is smaller by about 80 % than the one of the  
 09 well-known  $\text{SrAl}_2\text{O}_4:\text{Eu}^{2+}$ ,  $\text{Dy}^{3+}$ . Yang *et al.*<sup>10</sup> reported a significantly higher afterglow  
 10 intensity of  $\text{Ba}_4\text{Si}_6\text{O}_{16}:\text{Eu}^{2+}$ ,  $\text{Ho}^{3+}$ , well above those of previously reported  $\text{Ba}_4\text{Si}_6\text{O}_{16}:\text{Eu}^{2+}$ ,  $RE$   
 11 crystals and noticeably stronger than that of  $\text{SrAl}_2\text{O}_4:\text{Eu}^{2+}$ ,  $\text{Dy}^{3+}$ .

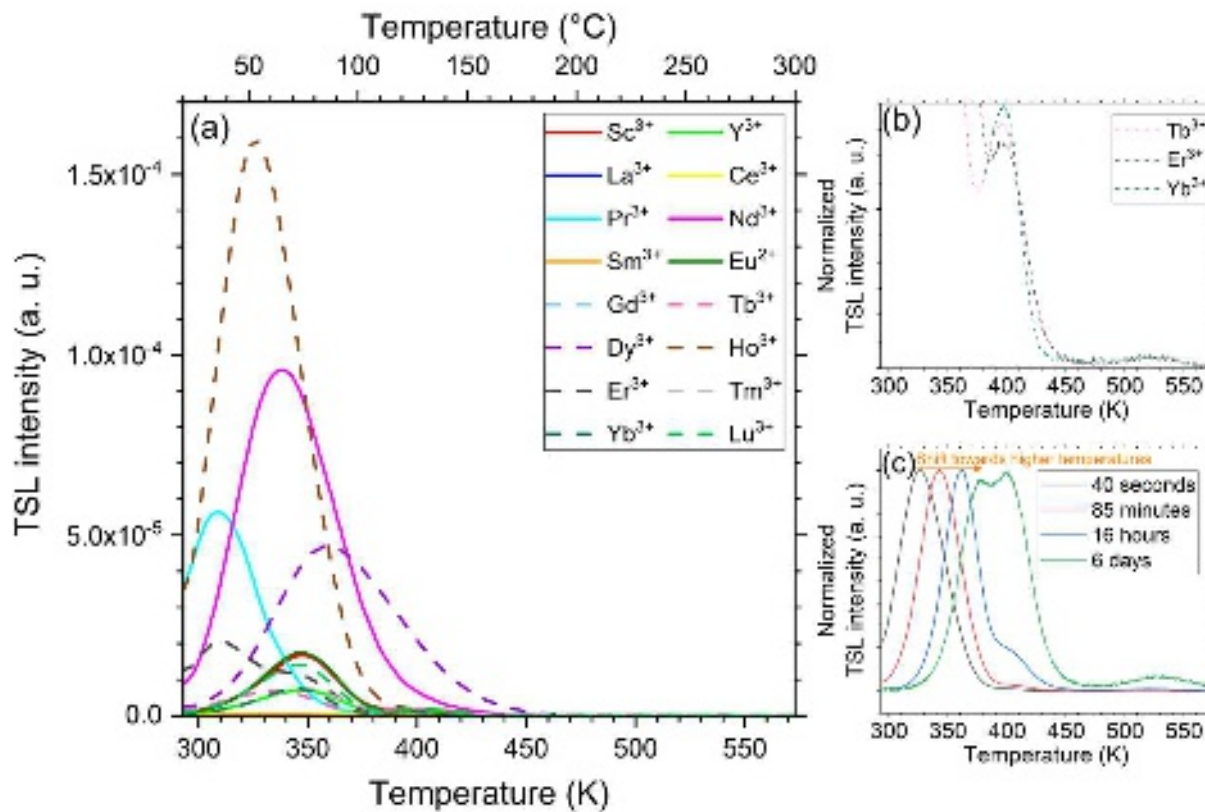


13 **FIG. 4.** Luminance of  $\text{Ba}_4\text{Si}_6\text{O}_{16}:\text{Eu}^{2+}$ , *RE* crystals reported here or in the literature<sup>10 32 33</sup>, as  
 14 well as that of well-known phosphors such as  $\text{Y}_3\text{Al}_2\text{Ga}_3\text{O}_{12}:\text{Ce}^{3+}$ ,  $\text{Yb}^{3+}$  (YAGG)<sup>35</sup>,  
 15  $\text{SrAl}_2\text{O}_4:\text{Eu}^{2+}$ ,  $\text{Dy}^{3+}$ <sup>36</sup>,  $\text{BaSi}_2\text{O}_2\text{N}_2:\text{Eu}^{2+}$ <sup>37</sup>. The *SSL* intensity of  $\text{Ba}_4\text{Si}_6\text{O}_{16}:\text{Eu}^{2+}$ ,  $\text{Ho}^{3+}$  is also  
 16 indicated.

17 *TSL* experiments provide key elements to better understand the *LLP* intensity and decay, such  
 18 as the trap depths and distributions. Trap depth  $E$  and concentration  $n_0$  can be calculated from  
 19 the *TSL* intensity  $I(T)$  according to<sup>38</sup>:

$$20 \quad I(T) = \left[ \left( \frac{(l-1)s}{\beta} \right) \times \int_{T_0}^T \exp\left(-\frac{E}{k_B T}\right) dT + 1 \right]^{-\frac{l}{l-1}} s n_0 \exp\left(-\frac{E}{k_B T}\right) \quad (2)$$

21 Where  $k_B$  is the Boltzmann constant,  $T$  the temperature,  $l$  the kinetic order,  $s$  the frequency  
 22 factor, and  $\beta$  the heating rate ( $1 \text{ K}\cdot\text{s}^{-1}$ ).  $E$ ,  $l$  and  $s$  were deduced according to previously  
 23 described methods<sup>39 40</sup>. *TSL* curves are plotted in FIG. 5 (a).



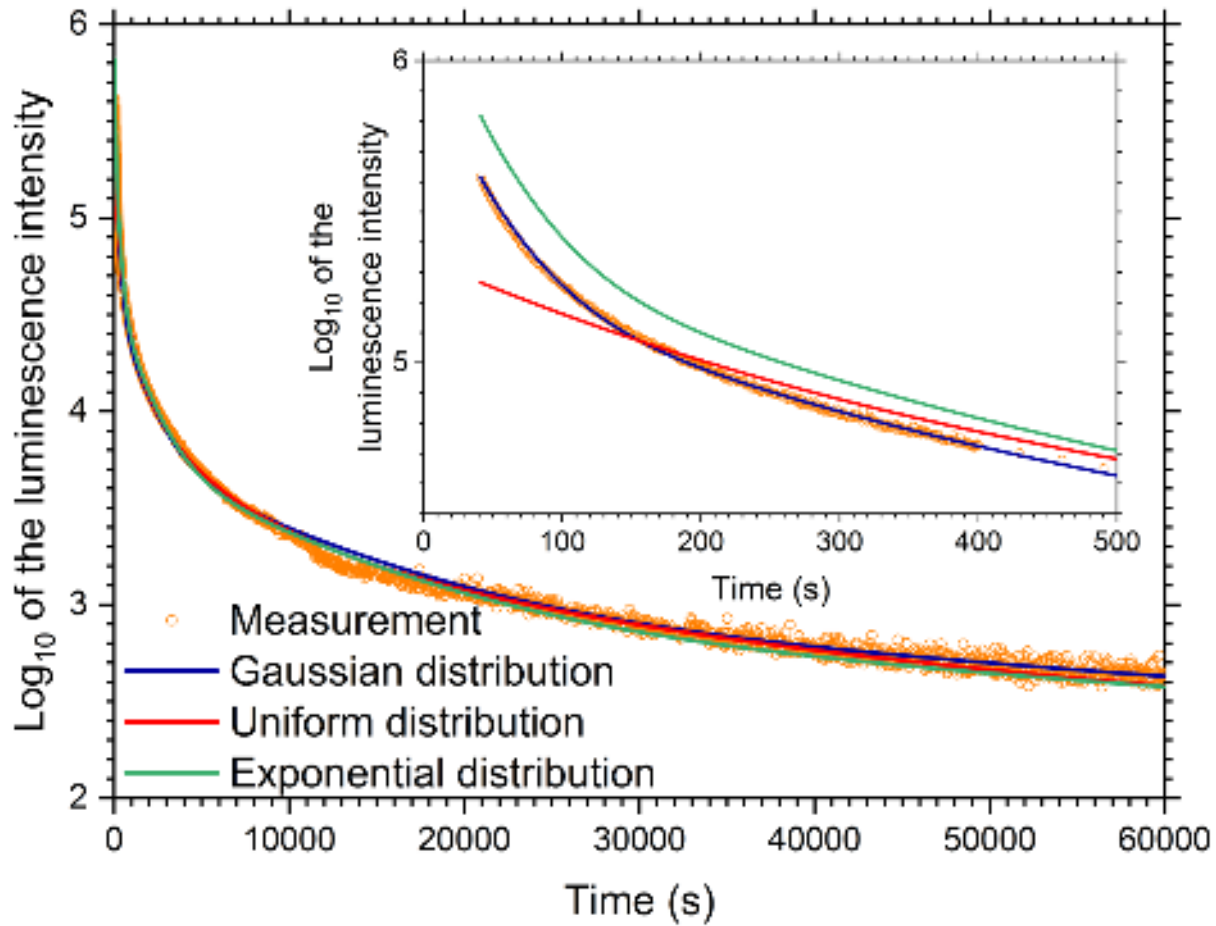
24

25 **FIG. 5.** (a) *TSL* measurements of  $\text{Ba}_4\text{Si}_6\text{O}_{16}:\text{Eu}^{2+}$ , *RE* crystals with a heating rate of  $1 \text{ K}\cdot\text{s}^{-1}$ .  
26 (b) Zoom-in of the *TSL* measurements highlighting the recurring 398 and 523 K *TSL* peaks (c)  
27 *TSL* measurements of  $\text{Ba}_4\text{Si}_6\text{O}_{16}:\text{Eu}^{2+}$ ,  $\text{Ho}^{3+}$  carried out with various delay times.

28 In  $\text{Ba}_4\text{Si}_6\text{O}_{16}:\text{Eu}^{2+}$ , *RE* crystals, three recurring *TSL* peaks were observed FIG. 5 (a) and FIG. 5  
29 (b). The first one lies in the 303-363 K region, while the second and third ones are  
30 systematically located at temperatures of 398 K and 523 K respectively. The only exceptions  
31 are i)  $\text{RE} = \text{Dy}^{3+}$ , for which the width of the first peak suggests two combined peaks ii)  $\text{Er}^{3+}$ ,  
32 which also exhibits two peaks in the 303-363 K region, and iii)  $\text{Tm}^{3+}$  that exhibits a third peak  
33 at 473 K. Such a recurrence in the peak position hints that the nature of those traps is similar  
34 regardless of the *RE* co-doping. Further experiments would be required to elucidate the physical  
35 and structural origins of these electron traps.

36 In addition, *TSL* experiments performed with different delay times with  $\text{RE} = \text{Ho}^{3+}$  evidenced  
37 a gradual shift from the first *TSL* peak towards higher temperatures FIG. 5 (c), which implies  
38 that at least for this co-dopant there is actually a distribution of trap depths rather than a discrete  
39 energy level. This is consistent with preliminary *DFT* calculations performed on the  $\text{Ba}_4\text{Si}_6\text{O}_{16}$   
40 crystal, which also show the presence of a distribution of energy levels arising from oxygen  
41 vacancies <sup>28</sup>. This distribution of energies would extend from at least  $E_{C_3} = 0.694$  to  
42  $E_{C_1} = 0.924$  eV, where  $C_3$  is the top and  $C_1$  the bottom of the trap distribution. It is slightly  
43 shallower than that reported by Yang *et al.* (which extended from 0.602 to 1.156 eV) <sup>10</sup>, where  
44 its deepness was possibly overestimated because of the close second *TSL* peak at 398 K. As a  
45 matter of fact, short (< 500 s) and long time (up to 60000 s) luminescence decay measured at  
46 the peak emission wavelength would suggest that this distribution is close to a gaussian form  
47 FIG. 6 <sup>41 42 43 44</sup>. It is noteworthy that *RE* co-doping in  $\text{Ba}_4\text{Si}_6\text{O}_{16}$  does not always lead to a

48 distribution of trap depths. For example, Dy<sup>3+</sup> co-doping does not induce a shift of the first *TSL*  
 49 peak position with increasing delay times <sup>10</sup>.

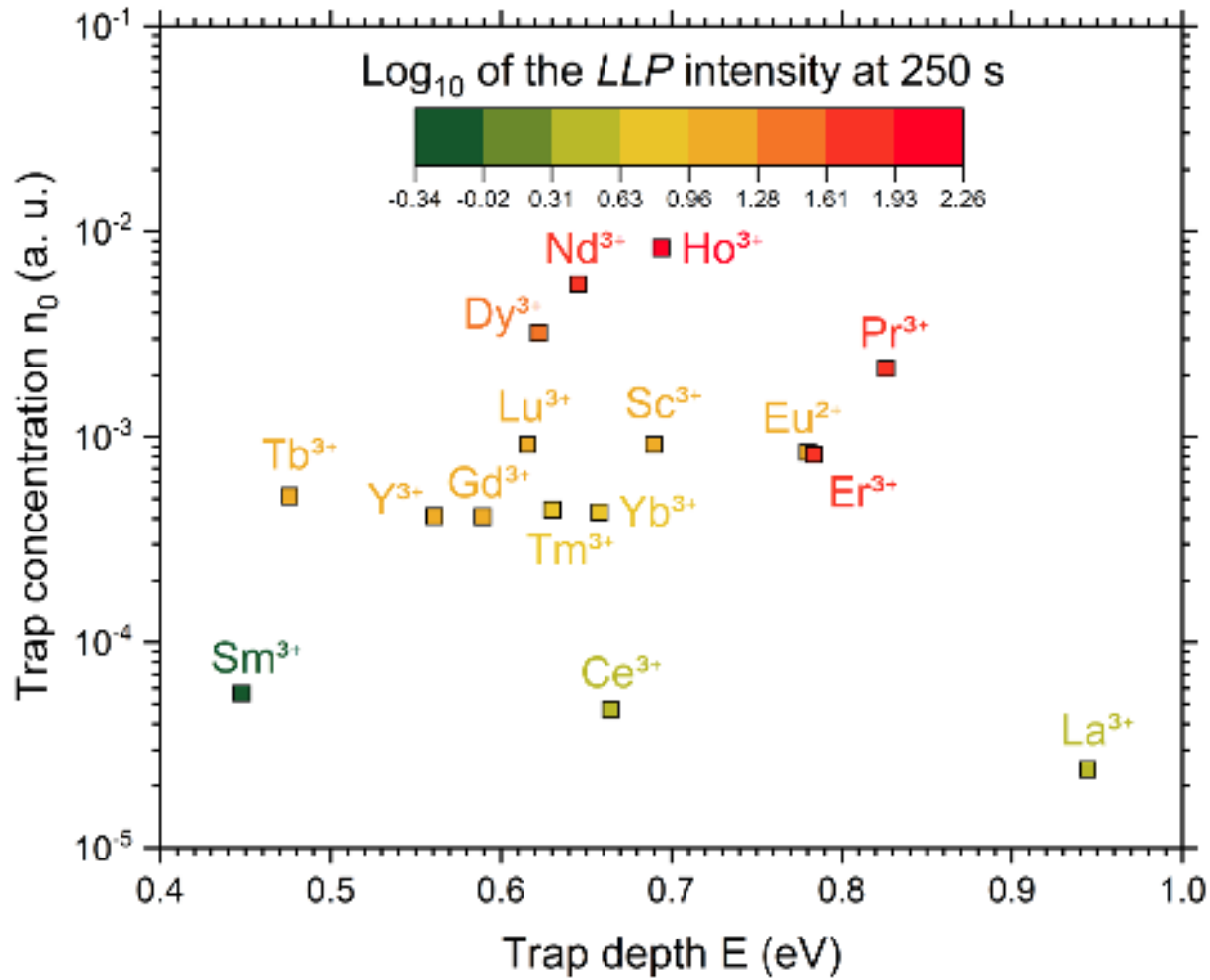


50 **FIG. 6.** *LLP* decay (< 60000 s) of Ba<sub>4</sub>Si<sub>6</sub>O<sub>16</sub>:Eu<sup>2+</sup>, Ho<sup>3+</sup> fitted with various distribution shapes.  
 51 The inset shows the *LLP* decay at short times (< 500 s).  
 52

53 In order to get more insight into the *LLP* behavior of Ba<sub>4</sub>Si<sub>6</sub>O<sub>16</sub>:Eu<sup>2+</sup>, RE crystals at the scale  
 54 of a few minutes, only traps with a depth of 1 eV at most need to be considered, which  
 55 correspond to the first peak in the 303-363 K region. Thus, the second and third peaks, which  
 56 correspond to deeper traps are excluded from this study. The high sensitivity camera used for  
 57 *LLP* experiments does not allow to quantify the luminescence intensity immediately after the  
 58 excitation source is stopped. Therefore, the luminescence intensity at an arbitrarily chosen time  
 59 of 250 s was used as a reflection of the *LLP* lifetime. As can be seen in FIG. 7, there is an



60 excellent agreement between the *LLP* behavior and the traps depths and concentrations as  
 61 determined from the spectra in FIG. 5 by means of equation (2): the  $\text{Ba}_4\text{Si}_6\text{O}_{16}:\text{Eu}^{2+}$ , *RE* crystals  
 62 with the strongest afterglow intensity are the ones with the largest concentrations of traps with  
 63 depths ranging from 0.65 to 0.85 eV, a region where the relaxation kinetics to the fundamental  
 64 state is of the order of a few minutes to several days.



65 **FIG. 7.** Trap depth and concentration of the various  $\text{Ba}_4\text{Si}_6\text{O}_{16}:\text{Eu}^{2+}$ , *RE* crystals determined  
 66 from equation (2).  
 67  
 68

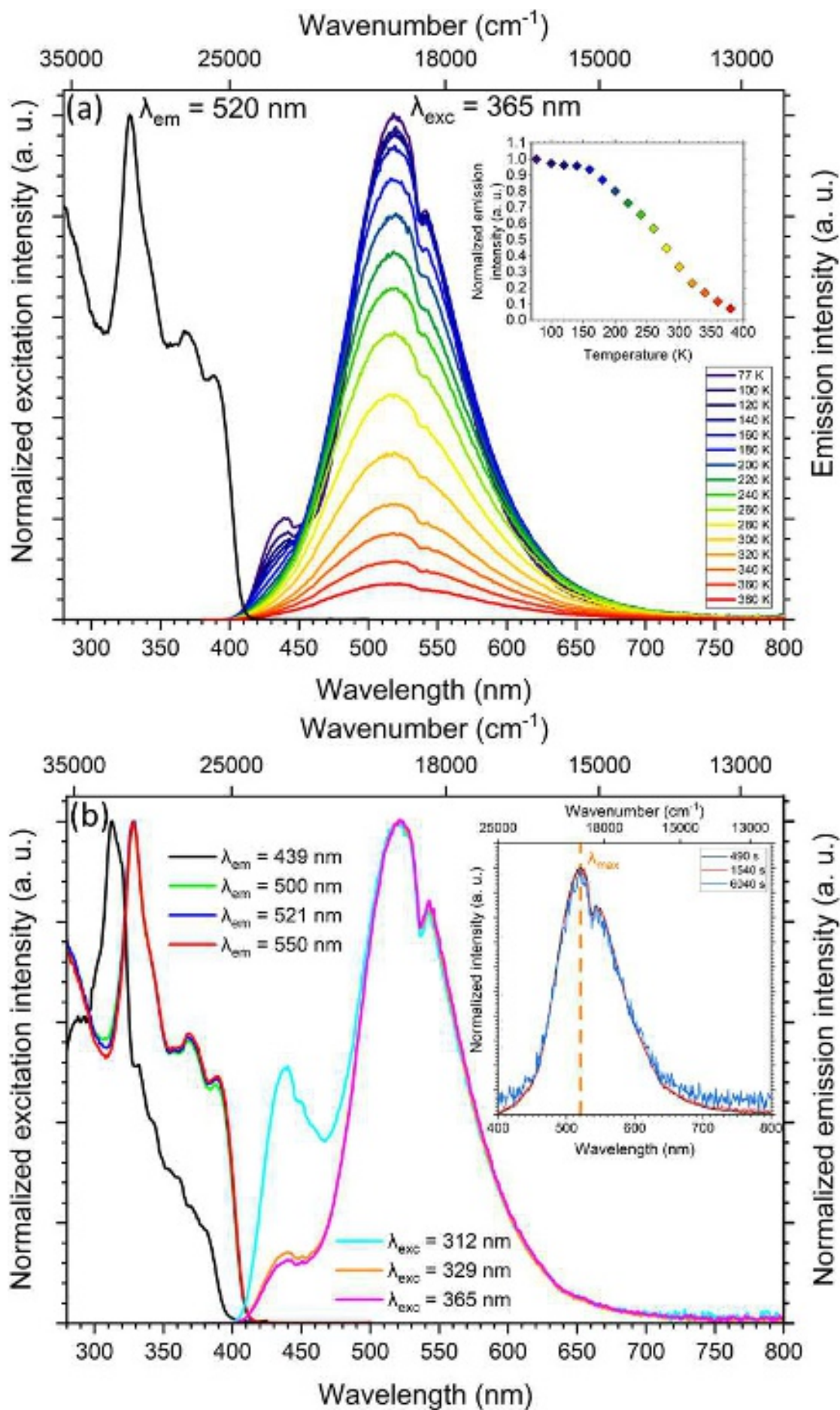
This is the author's peer reviewed, accepted manuscript. However, the online version of record will be different from this version once it has been copyedited and typeset. PLEASE CITE THIS ARTICLE AS DOI: 10.1063/5.0167222

69 **3.2 Eu(1) and Eu(2) emission bands**

70 As europium ions are incorporated in  $\text{Ba}_4\text{Si}_6\text{O}_{16}$  crystals,  $\text{Eu}^{2+}$  will occupy the two  
71 non-equivalent  $\text{Ba}^{2+}$  sites. It was proposed that, because both Ba(1) and Ba(2) sites are  
72 coordinated by eight oxygen atoms <sup>27</sup>, the two europium ions environments are relatively  
73 similar, in agreement with the fact that two broad emission bands with close emission maximum  
74 are observed <sup>7 10 32</sup>. Indeed, while the 4f electrons of divalent europium are quite insensitive to  
75 their surroundings, this is not the case of the 5d electrons <sup>32</sup>. Consistently, the broad emission  
76 band could be deconvoluted into two bands at  $\lambda_{max} = 500$  and 550 nm, corresponding to the  
77 two non-equivalent europium sites, namely Eu(1) and Eu(2) <sup>32</sup>. This is supported by i) a shift  
78 of the broad emission band maximum towards longer wavelength when the delay time  
79 increases, which suggests the existence of two different lifetimes for each site <sup>32</sup>, and ii) a  
80 significantly different excitation spectra when  $\lambda_{em} = 500$  or 550 nm.

81 Thermoluminescence experiments performed in this work from 77 to 380 K support another  
82 interpretation. When the emission spectra are measured at temperatures as low as 77 K, one can  
83 observe a second emission band appearing at  $\lambda_{max} = 439$  nm, in addition to the green emission  
84 band at  $\lambda_{max} = 521$  nm FIG. 8 (a). The intensity of this blue emission band gradually decreases  
85 up to 200 K where it is no longer visible, while the thermal quenching of the green emission  
86 band starts at 160 K but is not yet completed at 380 K. Furthermore, excitation spectra collected  
87 at 77 K with  $\lambda_{em} = 500$ , 521, or 550 nm are identical FIG. 8 (b), but all-three were notably  
88 different from the one obtained with  $\lambda_{em} = 439$  nm. Indeed, the latter is shifted towards shorter  
89 wavelengths and its behavior in the 330-400 nm region is clearly unlike. This is in  
90 contradiction with what was previously reported <sup>32</sup>. This suggests that i) the blue and green  
91 emission bands are of different nature, which is clearly outlined when  $\lambda_{exc} = 312$  nm, and ii)  
92 the green emission band is not composed of two subsequent emission bands.

This is the author's peer reviewed, accepted manuscript. However, the online version of record will be different from this version once it has been copyedited and typeset.  
PLEASE CITE THIS ARTICLE AS DOI: 10.1063/1.5016722



94 **FIG. 8.** (a) Excitation spectra measured at 77 K and emission spectra measured at various  
95 temperatures (20 K steps) of  $\text{Ba}_4\text{Si}_6\text{O}_{16}:\text{Eu}^{2+}, \text{Ho}^{3+}$ . The inset shows the emission intensity at  
96 various temperatures. (b) Excitation and emission spectra of  $\text{Ba}_4\text{Si}_6\text{O}_{16}:\text{Eu}^{2+}, \text{Ho}^{3+}$  at 77 K. The  
97 inset shows the *LLP* emission spectra at ambient temperature various times after the excitation  
98 source is stopped.

99 The interpretation proposed in this work is supported by emission spectra measured at various  
100 times after the excitation source is stopped, where no shift of the emission maximum was  
101 observed FIG. 8 (b), which was already noted in another study<sup>45</sup>. The previously observed shift  
102 is likely resulting from the presence of  $\beta\text{-BaSiO}_3$  as a secondary phase, which is revealed by  
103 the presence of a peak on the *XRD* pattern at  $26^\circ$  FIG. 1. The persistent luminescence properties  
104 of this crystal are known<sup>11</sup> and an emission maximum at  $\lambda_{max} = 560$  nm was identified, which  
105 explains the shift of the emission maximum towards longer wavelengths with time.

106 It is thus concluded that the two non-equivalent  $\text{Eu}^{2+}$  sites are sufficiently different to give birth  
107 to two emission bands at low temperatures. Indeed, the Ba(1) polyhedron is more distorted than  
108 the Ba(2) one<sup>27</sup>, so that an 82 nm difference between the two emission bands maximum is  
109 observed. It was proposed that the higher distortion degree of the Ba(1) polyhedra would result  
110 in a weaker crystal field of Ba(1) than that of Ba(2)<sup>10</sup>, thus, the broad emission band of Eu(1)  
111 would be in a shorter wavelength region than that of Eu(2)<sup>46</sup>, *i. e.* the blue emission band would  
112 correspond to Eu(1) and the green one to Eu(2). However, it is still not clear as to why the  
113 thermal quenching of Eu(1) occurs at much lower temperatures than that of Eu(2).

114 The thermoluminescence behavior of  $\text{Ba}_4\text{Si}_6\text{O}_{16}:\text{Eu}^{2+}, \text{Ho}^{3+}$  is very similar to that of monoclinic  
115  $\text{SrAl}_2\text{O}_4:\text{Eu}^{2+}, \text{Dy}^{3+}$ . In the latter, a blue emission band also appears at low temperatures  
116 ( $\lambda_{max} = 445$  nm) which arises from the presence of two non-equivalent  $\text{Sr}^{2+}$  sites in the crystal  
117 structure<sup>47</sup>. In addition, the asymmetric green emission band of  $\text{Ba}_4\text{Si}_6\text{O}_{16}:\text{Eu}^{2+}, \text{Ho}^{3+}$  is shifted

18 to larger wavelengths just like the green emission band ( $\lambda_{max} = 520$  nm) of strontium  
19 aluminate. In this latter case, this was discussed by Botterman *et al.*<sup>47</sup> in terms of the centroid  
20 shift and crystal field splitting.

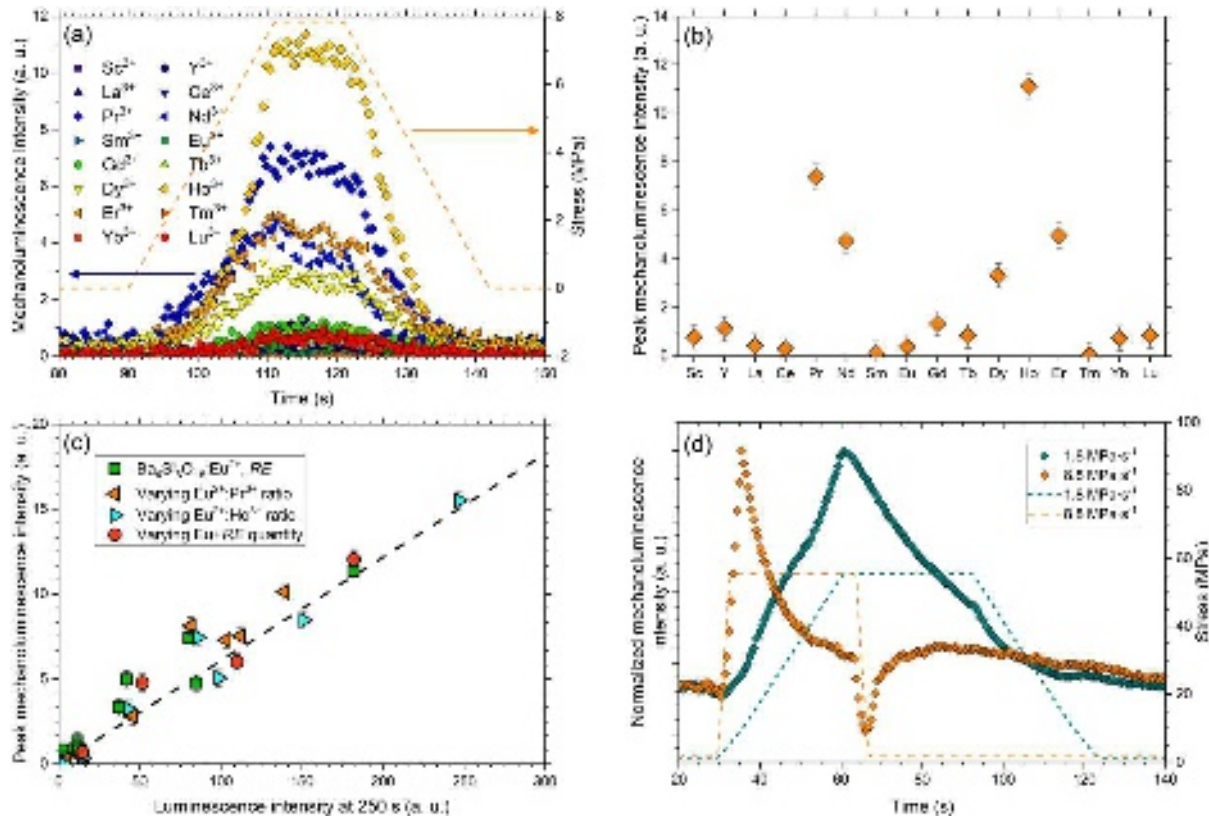
21

### 22 3.3 Mechanoluminescence properties of $\text{Ba}_4\text{Si}_6\text{O}_{16}:\text{Eu}^{2+}$ , *RE*

23 The *EML* response of  $\text{Ba}_4\text{Si}_6\text{O}_{16}:\text{Eu}^{2+}$ , *RE*/epoxy composites, obtained by subtracting the *LLP*  
24 intensity as recorded at rest (*i. e.* at  $\sigma = 0$  MPa) to the mechanically-loaded specimen, was  
25 characterized by means of the diametral compression tests FIG. 9 (a). Each test was performed  
26 with a  $0.37 \text{ MPa}\cdot\text{s}^{-1}$  stress rate. It is recalled that the *EML* intensity is proportional to both the  
27 stress and the stress rate<sup>48</sup>. In a similar way as with the previous *LLP* measurements, the *RE*  
28 co-doping has a pronounced effect on the intensities of the *EML* signal. The largest intensities  
29 are obtained with *RE* =  $\text{Ho}^{3+}$ ,  $\text{Pr}^{3+}$ ,  $\text{Er}^{3+}$ , or  $\text{Nd}^{3+}$  FIG. 9 (b). The mechanical stress was applied  
30 90 s after the excitation source was stopped, as longer delays resulted in smaller *EML* intensity.  
31 This suggests that the charge carriers involved in the *EML* of  $\text{Ba}_4\text{Si}_6\text{O}_{16}:\text{Eu}^{2+}$ , *RE* crystals  
32 slowly recombine with the luminescent center with time, and are thus also participating in the  
33 *LLP* at the scale of several minutes/hours.

34 There seems to be a strong connection between the *EML* intensity and the *LLP* intensity FIG. 9  
35 (c). Various mechanisms were proposed to explain the mechanically-induced luminescence<sup>29</sup>,  
36 among which those involving piezoelectricity are the most popular. It is supposed that, as a  
37 stress field is applied, the trap depths are changed thanks to piezoelectricity, ultimately altering  
38 the charge carriers recombination kinetics. Although  $\text{Ba}_4\text{Si}_6\text{O}_{16}$  is centrosymmetric (space  
39 group  $P2_1/c$ ) and should therefore not exhibit piezoelectricity, centrosymmetry might be broken  
40 at the local scale by the presence of defects, so that piezoelectricity can subsequently be  
41 observed<sup>29</sup>. In  $\text{Ba}_2\text{Si}_2\text{O}_2\text{N}_2:\text{Eu}^{2+}$ , the stress is assumed to induce a decrease of a trap depth

42 leading to an increased luminescence intensity<sup>20</sup>. In the  $\text{SrAl}_2\text{O}_4:\text{Eu}^{2+}$ ,  $\text{Dy}^{3+}$  compound, a  
 43 mechanism with three discrete traps allowed to explain an increase in the luminescence  
 44 intensity both during the loading and the unloading stages<sup>49</sup>. This correlation is therefore  
 45 consistent with this latter mechanism: a larger trap concentration with depths ranging from 0.65  
 46 to 0.85 eV is assumed i) to result in a stronger *LLP* intensity, but also ii) in a stronger *EML*  
 47 intensity, as more charge carriers will be able to recombine with the luminescent center when  
 48 the trap depth decreases.



49 PLEASE CITE THIS ARTICLE AS DOI: 10.1063/1.5167222  
 50 **FIG. 9.** (a) *EML* intensity of  $\text{Ba}_4\text{Si}_6\text{O}_{16}:\text{Eu}^{2+}$ , RE/epoxy composites (b) Peak *EML* intensity of  
 51  $\text{Ba}_4\text{Si}_6\text{O}_{16}:\text{Eu}^{2+}$ , RE/epoxy composites (c) Peak *EML* intensity plotted as a function of the  
 52 luminescence intensity at 250 s (d) *EML* intensity of  $\text{Ba}_4\text{Si}_6\text{O}_{16}:\text{Eu}^{2+}$ ,  $\text{Ho}^{3+}$ /epoxy composite  
 53 with stress rates of 1.8 and 8.8  $\text{MPa}\cdot\text{s}^{-1}$ .

54 Regarding the  $\text{Ba}_4\text{Si}_6\text{O}_{16}:\text{Eu}^{2+}$ ,  $\text{Ho}^{3+}$  compound, its *EML* behavior contrasts with the one of  
 55  $\text{SrAl}_2\text{O}_4:\text{Eu}^{2+}$ ,  $\text{Dy}^{3+}$ . It is particularly outlined with high stress rates (here with 8.8  $\text{MPa}\cdot\text{s}^{-1}$ ),

56 where *EML* is more intense and therefore better resolved FIG. 9 (d). It is noteworthy that the  
57 *EML* behavior of the Ba<sub>4</sub>Si<sub>6</sub>O<sub>16</sub>:Eu<sup>2+</sup>, Ho<sup>3+</sup>/epoxy composite is identical to that of a  
58 mechanoluminescent glass-ceramic with the same cationic composition <sup>28</sup>. The mechanical  
59 loading and its holding lead to an increase in the luminescence intensity, while the unloading  
60 leads to a decrease of the luminescence intensity. Changes in irradiation time lead to an increase  
61 in both the luminescence and the mechanoluminescence intensity.

62 In particular, *TSL* experiments provide insight into the *EML* mechanism. Based on the existence  
63 of an electron trap distribution, we can propose an energy level scheme for  
64 Ba<sub>4</sub>Si<sub>6</sub>O<sub>16</sub>:Eu<sup>2+</sup>, Ho<sup>3+</sup> FIG. 10. Although the identified charge carriers (holes and/or electrons)  
65 involved in the afterglow of Ba<sub>4</sub>Si<sub>6</sub>O<sub>16</sub>:Eu<sup>2+</sup>, *RE* phosphors are still unknown <sup>32</sup>, it is assumed  
66 that electrons are the key players. Traps corresponding to the 398 K and 523 K *TSL* peaks are  
67 too deep to contribute to the *EML* effect. The Eu<sup>2+</sup> ions electronic configuration changes from  
68 the ground state 4f<sup>7</sup> to the 4f<sup>6</sup>5d<sup>1</sup> excited state under UV light. Then, the electron can escape to  
69 the conduction band and eventually reaches energy levels located in the band gap, leaving  
70 behind Eu<sup>3+</sup> ions. The main effect of the mechanical loading is to change the depth of the trap  
71 distribution, *i. e.* the *C*<sub>3</sub> and/or the *C*<sub>1</sub> trap depth decreases (FIG. 10 illustrates the scenario  
72 where the depth of the whole trap distribution decreases). The recombination probability is  
73 therefore higher and an increase of the luminescence intensity follows. However, the  
74 mechanical loading empties the stocked charge carriers at a much higher rate than it would have  
75 at rest. As a matter of fact, a smaller luminescence intensity is observed after the stress is  
76 relieved. This model provides an explanation to the observed *EML* during both mechanical  
77 loading and unloading, in consistency i) with the *EML* mechanisms involving changes in trap  
78 depths through piezoelectricity, and ii) the decrease in the *EML* intensity with long delays prior  
79 to mechanical loading in Ba<sub>4</sub>Si<sub>6</sub>O<sub>16</sub>:Eu<sup>2+</sup>, *RE* crystals.

This is the author's pre-proof, peer-reviewed, and accepted manuscript. It may differ from the final version of the record. For more information, please refer to the AIP Publishing website. This is the author's pre-proof, peer-reviewed, and accepted manuscript. It may differ from the final version of the record. For more information, please refer to the AIP Publishing website.

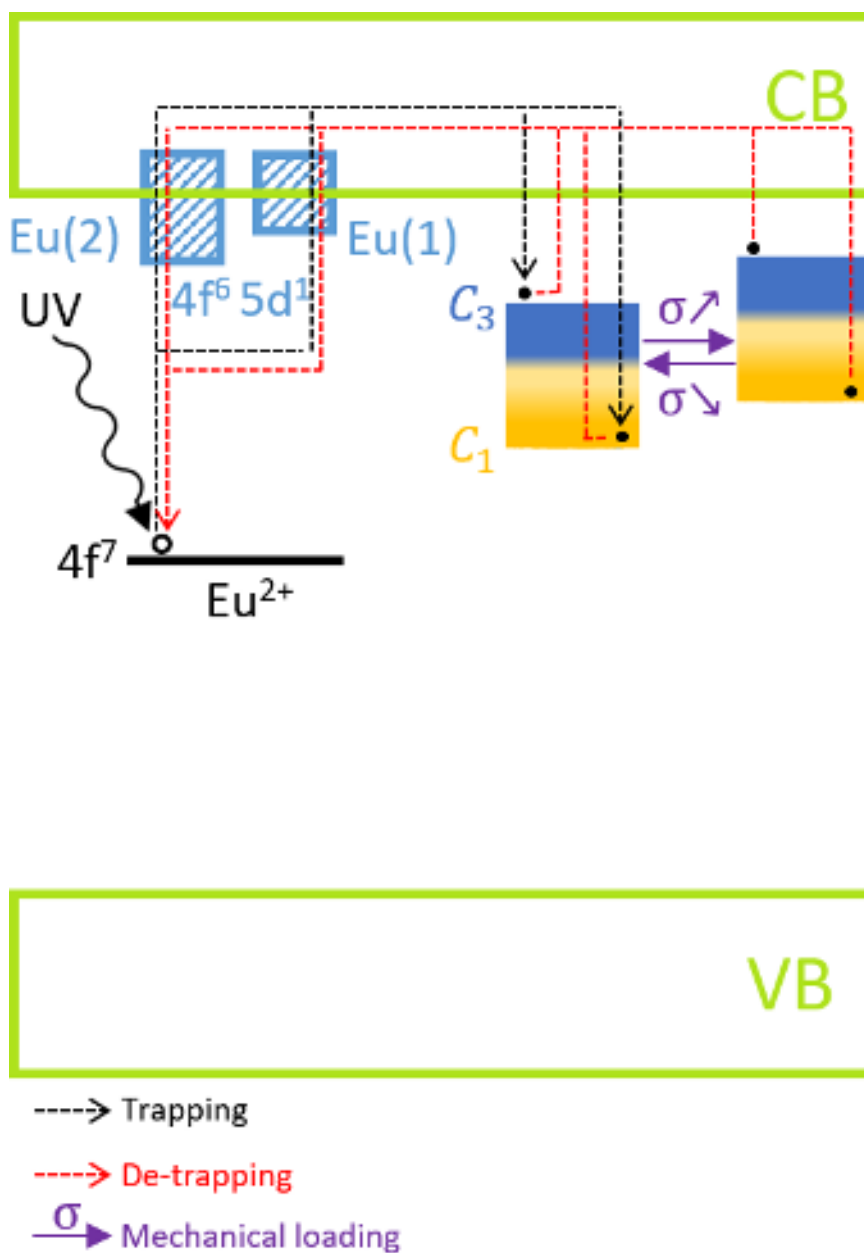


**FIG. 10.** Energy level scheme of  $\text{Ba}_4\text{Si}_6\text{O}_{16}:\text{Eu}^{2+}$ ,  $\text{Ho}^{3+}$  under mechanical stress. For the sake of clarity, the trap distribution is shown as a continuous succession of trap depths.

#### 4. CONCLUSION

The luminescence properties of  $\text{Ba}_4\text{Si}_6\text{O}_{16}:\text{Eu}^{2+}$ ,  $\text{RE}$  crystals, as well as their  $EML$  properties, were studied. A change in the  $\text{RE}$  co-doping leads to small changes in the emission wavelength, but to dramatic changes in the  $LLP$  behavior and  $EML$  intensity. The incidence of the  $\text{RE}$



88 co-doping was put into perspectives with trap depths and concentrations determined from *TSL*  
89 measurements. Exact definition of co-doping and  $\text{Eu}^{2+}$  concentration allows to tune the  
90 emission color and lifetime of  $\text{Ba}_4\text{Si}_6\text{O}_{16}:\text{Eu}^{2+}$ , *RE* phosphors. When  $RE = \text{Ho}^{3+}$ , the *LLP*  
91 duration extends beyond a day.

92 Emission spectra measured at low temperatures revealed a second emission band  
93 ( $\lambda_{max} = 439$  nm) in addition to the green emission band ( $\lambda_{max} = 521$  nm). They stem from  $\text{Eu}^{2+}$   
94 ions located in the two non-equivalent  $\text{Ba}^{2+}$  sites in  $\text{Ba}_4\text{Si}_6\text{O}_{16}$ , in a similar way as in  
95  $\text{SrAl}_2\text{O}_4:\text{Eu}^{2+}$ ,  $\text{Dy}^{3+}$ .

96 *TSL* experiments unveiled a trap distribution from 0.694 to 0.924 eV in  $\text{Ba}_4\text{Si}_6\text{O}_{16}:\text{Eu}^{2+}$ ,  $\text{Ho}^{3+}$   
97 that allowed, with *EML* experiments, to build an energy level scheme of the ongoing *EML*  
98 mechanism. Mechanical loading decreases the depth of the trap distribution, resulting in a faster  
99 release of the charge carriers and ultimately in an increase of the luminescence intensity. During  
00 unloading, the trap distribution returns to its initial position but with significantly less charge  
01 carriers, which is exhibited by a drop of the luminescence intensity *i. e.* by a negative *EML*  
02 intensity.

## 04 ACKNOWLEDGEMENTS

05 We acknowledge financial support from Région Bretagne and from the European Research  
06 Council (ERC Adv. Grant “DAMREG”).

## 08 AUTHOR DECLARATIONS

09 **Conflict of Interest**

10 The authors have no conflicts to disclose.

11

## 12 **Author Contributions**

13 **Alexis Duval:** Conceptualization (lead); Data curation (lead); Investigation (lead);  
14 Methodology (lead); Writing – original draft (lead). **Yan Suffren:** Conceptualization (equal);  
15 Data curation (lead); Investigation (equal); Methodology (equal); Writing – review & editing  
16 (equal). **Mourad Benabdesselam:** Conceptualization (equal); Data curation (lead);  
17 Investigation (equal); Methodology (equal); Writing – review & editing (equal). **Patrick**  
18 **Houizot:** Conceptualization (equal); Investigation (equal); Methodology (equal); Supervision  
19 (equal); Writing – review & editing (equal). **Tanguy Rouxel:** Conceptualization (equal);  
20 Methodology (equal); Supervision (equal); Writing – review & editing (equal).

## 21 **DATA AVAILABILITY**

22 The data that support the findings of this study are available within the article and from the  
23 corresponding author upon reasonable request.

## 24 **ORCID**

25 Alexis Duval iD <https://orcid.org/0000-0001-9192-2454>

26 Yan Suffren iD <https://orcid.org/0000-0001-6338-8274>

27 Mourad Benabdesselam iD <https://orcid.org/0000-0002-9207-2938>

28 Patrick Houizot iD <https://orcid.org/0000-0002-6360-6996>

29

30

This is the author's peer-reviewed accepted manuscript. However, the only version of record for this version is the final version that has been copyedited and typeset. PLEASE CITE THIS ARTICLE AS DOI: 10.1063/5.0167222

31 Tanguy Rouxel iD <https://orcid.org/0000-0002-9961-245>

32

33 **REFERENCES**

34 <sup>1</sup> X. Meng, H. Li, Z. Wang, Y. Li, H. Lin, S. Liu, and Y. He, *Mater. Lett.* **297**, 129928 (2021).

35 <sup>2</sup> C. Donghua, W. Hui, W. Hongjun, and Y. Weiqiang, *J. Semicond.* **36**, (2015).

36 <sup>3</sup> R. Zhang, T. Maeda, R. Maruta, S. Kusaka, B. Ding, K. ichiro Murai, and T. Moriga, *J.*  
37 *Solid State Chem.* **183**, 620 (2010).

38 <sup>4</sup> Z. Dong, Y. Qin, Y. Yang, D. Zhou, X. Xu, and J. Qiu, *J. Rare Earths* **34**, 453 (2016).

39 <sup>5</sup> P. Wang, X. Xu, D. Zhou, X. Yu, and J. Qiu, *Inorg. Chem.* **54**, 1690 (2015).

40 <sup>6</sup> I.S. Cho, D.K. Yim, C.H. Kwak, J.S. An, H.S. Roh, and K.S. Hong, *J. Lumin.* **132**, 375  
41 (2012).

42 <sup>7</sup> Y. Li, Y. Fang, N. Hirosaki, R.J. Xie, L. Liu, T. Takeda, and X. Li, *Materials (Basel)*. **3**,  
43 1692 (2010).

44 <sup>8</sup> M. Chen, Z. Xia, M.S. Molokeev, and Q. Liu, *J. Mater. Chem. C* **3**, 12477 (2015).

45 <sup>9</sup> W.-S. Song, H.-J. Kim, Y.-S. Kim, and H. Yang, *J. Electrochem. Soc.* **157**, J319 (2010).

46 <sup>10</sup> Z. Yang, Y. Hu, L. Chen, and X. Wang, *Opt. Mater. (Amst)*. **35**, 1264 (2013).

47 <sup>11</sup> Y. Jia, W. Sun, R. Pang, T. Ma, D. Li, H. Li, S. Zhang, J. Fu, L. Jiang, and C. Li, *Mater.*  
48 *Des.* **90**, 218 (2016).

49 <sup>12</sup> X. Li, Y. Liang, F. Yang, Z. Xia, W. Huang, and Y. Li, *J. Mater. Sci. Mater. Electron.* **24**,  
50 3199 (2013).

This is the author's pre-proof version of the manuscript. However, the online version of the article will differ from this version since it has been edited and typeset. PLEASE CITE THIS ARTICLE AS DOI: 10.1063/5.0167222

- 51 <sup>13</sup> M. Zhang, J. Wang, Q. Zhang, W. Ding, and Q. Su, **42**, 33 (2007).
- 52 <sup>14</sup> D. Kim, T.H. Kim, T.E. Hong, J. Bae, C.H. Kim, J. Kim, S. Kim, K. Jeon, and J. Park,  
53 *Materials (Basel)*. **13**, 1859 (2020).
- 54 <sup>15</sup> K. Asami, J. Ueda, K. Yasuda, K. Hongo, R. Maezono, M.G. Brik, and S. Tanabe, *Opt.*  
55 *Mater. (Amst)*. **84**, 436 (2018).
- 56 <sup>16</sup> M. Yamaga, Y. Masui, S. Sakuta, N. Kodama, and K. Kaminaga, *Phys. Rev. B - Condens.*  
57 *Matter Mater. Phys.* **71**, 1 (2005).
- 58 <sup>17</sup> M. Yamaga, Y. Masui, and N. Kodama, *Opt. Mater. (Amst)*. **36**, 1776 (2014).
- 59 <sup>18</sup> J.K. Park, M.A. Lim, K.J. Choi, and C.H. Kim, *J. Mater. Sci.* **40**, 2069 (2005).
- 60 <sup>19</sup> S.H. Choi, S. Bin Kwon, U. Bin Humayoun, W.K. Park, K. Toda, M. Kakihana, T. Masaki,  
61 W.S. Yang, Y.H. Song, and D.H. Yoon, *Dye. Pigment*. **148**, 460 (2018).
- 62 <sup>20</sup> J. Botterman, K. Van Den Eeckhout, I. De Baere, D. Poelman, and P.F. Smet, *Acta Mater.*  
63 **60**, 5494 (2012).
- 64 <sup>21</sup> H. Pan, D. Luo, L. Wang, and Y. Li, *Int. Conf. Manuf. Sci. Eng. (ICMSE 2015)* 690  
65 (2015).
- 66 <sup>22</sup> B. Wang, J. Chen, Y. Xia, and Y. Liu, *J. Nanosci. Nanotechnol.* **16**, 3608 (2016).
- 67 <sup>23</sup> P.F. Smet, J. Botterman, K. Van Den Eeckhout, K. Korthout, and D. Poelman, *Opt. Mater.*  
68 (Amst). **36**, 1913 (2014).
- 69 <sup>24</sup> F. Xiao, Y.N. Xue, and Q.Y. Zhang, *Spectrochim. Acta - Part A Mol. Biomol. Spectrosc.*  
70 **74**, 758 (2009).
- 71 <sup>25</sup> W. Peng-Jiu, X. Xu-Hui, Q. Jian-Bei, Z. Da-Cheng, L. Xue-E, and C. Shuai, *Acta Phys.*

This is the author's peer-reviewed, accepted manuscript. However, the online version of the record will be different from the published version. Please cite this article as DOI: 10.1063/1.5016722

- 72 Sin. **63**, 077804 (2014).
- 73 <sup>26</sup> R.D. Shannon, Acta Crystallogr. Sect. A **32**, 751 (1976).
- 74 <sup>27</sup> K.-F. Hesse and F. Liebau, Zeitschrift Für Krist. **153**, 3 (1980).
- 75 <sup>28</sup> A. Duval, P. Houizot, X. Rocquefelte, and T. Rouxel, Appl. Phys. Lett. **123**, 011905  
76 (2023).
- 77 <sup>29</sup> A. Feng and P.F. Smet, Materials (Basel). **11**, 484 (2018).
- 78 <sup>30</sup> C. Lara, M.J. Pascual, and A. Durán, J. Non. Cryst. Solids **348**, 149 (2004).
- 79 <sup>31</sup> N. Claussen and J. Jahn, Powder Metall. International **2**, 87 (1970).
- 80 <sup>32</sup> Y. Gong, Y. Wang, Y. Li, X. Xu, and W. Zeng, Opt. Express **19**, 4310 (2011).
- 81 <sup>33</sup> P. Wang, X. Xu, J. Qiu, X. Yu, and Q. Wang, Opt. Mater. (Amst). **36**, 1826 (2014).
- 82 <sup>34</sup> G.H. Dieke and H.M. Crosswhite, Appl. Opt. **2**, 675 (1963).
- 83 <sup>35</sup> J. Ueda, Bull. Chem. Soc. Jpn. **94**, 2807 (2021).
- 84 <sup>36</sup> A. Nag and T.R.N. Kutty, J. Alloys Compd. **354**, 221 (2003).
- 85 <sup>37</sup> J. Botterman, K. Van den Eeckhout, A.J.J. Bos, P. Dorenbos, and P.F. Smet, Opt. Mater.  
86 Express **2**, 341 (2012).
- 87 <sup>38</sup> R. Chen and Y. Kirsh, Int. Ser. Sci. Solid State **15**, 17 (1981).
- 88 <sup>39</sup> R. Chen, J. Electrochem. Soc. **116**, 1254 (1969).
- 89 <sup>40</sup> M.S. Jahan, D.W. Cooke, W.L. Hults, J.L. Smith, B.L. Bennett, and M.A. Maez, J. Lumin.  
90 **47**, 85 (1990).
- 91 <sup>41</sup> J.T. Randall and M.H.F. Wilkins, Proc. R. Soc. London. Ser. A. Math. Phys. Sci. **184**, 365

- 92 (1945).
- 93 <sup>42</sup> J.T. Randall and M.H.F. Wilkins, Proc. R. Soc. London. Ser. A. Math. Phys. Sci. **184**, 390
- 94 (1945).
- 95 <sup>43</sup> W.F. Hornyak and R. Chen, J. Lumin. **44**, 73 (1989).
- 96 <sup>44</sup> W.L. Medlin, Phys. Rev. **123**, 502 (1961).
- 97 <sup>45</sup> X. Zhang, X. Xu, Q. He, J. Qiu, and X. Yu, ECS J. Solid State Sci. Technol. **2**, R225
- 98 (2013).
- 99 <sup>46</sup> G. Blasse and B.C. Grabmaier, Springer (1994).
- 00 <sup>47</sup> J. Botterman, J.J. Joos, and P.F. Smet, Phys. Rev. B - Condens. Matter Mater. Phys. **90**, 1
- 01 (2014).
- 02 <sup>48</sup> M. Dubernet, Y. Gueguen, P. Houizot, F. Célarié, J.C. Sangleboeuf, H. Orain, and T.
- 03 Rouxel, Appl. Phys. Lett. **107**, 151906 (2015).
- 04 <sup>49</sup> M. Dubernet, E. Bruyer, Y. Gueguen, P. Houizot, J.C. Hameline, X. Rocquefelte, and T.
- 05 Rouxel, Sci. Rep. **10**, 19495 (2020).
- 06

This is the author's peer reviewed, accepted manuscript. However, the online version of record will be different from this version as it has been copyedited and typeset.  
PLEASE CITE THIS ARTICLE AS DOI: 10.1063/5.0167222